Ionics (2016) 22:2037–2044
DOI 10.1007/s11581-016-1736-8

ORIGINAL PAPER

Preparation of $LiNi_{0.5}Mn_{1.5}O_4$ cathode materials by electrospinning

Shengkui Zhong[1] · **Piao Hu**[1] · **Xia Luo**[1] · **Xiaoping Zhang**[1] · **Ling Wu**[1]

Received: 22 March 2016 / Revised: 23 April 2016 / Accepted: 10 May 2016 / Published online: 25 May 2016

Abstract $LiNi_{0.5}Mn_{1.5}O_4$ cathode material was prepared by electrospinning using lithium hydroxide, manganese acetate, nickel acetate, acetic acid, ethanol, and poly(vinyl pyrrolidone) as raw materials. The effect of calcination temperature on the structure, morphology, and electrochemical properties was investigated. XRD results indicate that the $LiNi_{0.5}Mn_{1.5}O_4$ composite is well crystallized as a spinel structure at calcination temperature of 650 °C for 3 h. SEM results reveal that this composite has a nanofiber shape with average size of about 300–500 nm. Electrochemical performance tests reveal that this composite shows the initial discharge capacity of 127.8 and 105 $mAhg^{-1}$ at 0.1 and 3 C rates, respectively, and exhibits good cycling performance.

Keywords Cathode material · $LiNi_{0.5}Mn_{1.5}O_4$ · Electrospinning · Nanofiber

Introduction

In order to satisfy the requirements of high energy density and working voltage of Li-ion batteries for electric vehicles (EVs), hybrid electric vehicles(HEVs), and communication engineering, cathode materials with high operating potentials(>4.5 V vs. Li/Li^+) have attracted amounts of attention in the current Li-ion battery industry.

The most wildly used cathode materials for the present commercialized lithium-ion batteries are $LiCoO_2$, $LiFePO_4$, and $LiMn_2O_4$. But $LiCoO_2$ and $LiFePO_4$ have different limitations and disadvantages during their use. $LiCoO_2$ is difficult to be widely applied in the field of power battery due to its high cost and the toxicity of cobalt. $LiFePO_4$ is hard to satisfy the requirements of large energy storage systems because of its small tap density and low discharge voltage. Spinel $LiMn_2O_4$ is one of the most promising cathode material due to low cost, abundant resources, and nontoxicity [1, 2]. However, the spinel $LiMn_2O_4$ electrode suffers from a poor cycling behavior and severe capacity fading at elevated temperature [3, 4]. To improve the cycling performance and suppress capacity fading, Liu et al. [5] enhance the electrochemical performance of the $LiMn_2O_4$ hollow microsphere cathode with a $LiNi_{0.5}Mn_{1.5}O_4$ coated layer. Metal doping method has also been applied to synthesis spinel $LiM_xMn_{2-x}O_4$ (M=Ni, Mg, Co, Fe) [6, 7]. Among all possible compositions, $LiNi_{0.5}Mn_{1.5}O_4$ is the most attractive material with a typical capacity more than 135 $mAhg^{-1}$ (≥92 % of theoretical value) and a plateau voltage of capacity at around 4.7 V [8, 9].

A variety of synthetic methods for the preparation of $LiNi_{0.5}Mn_{1.5}O_4$ have been reported, such as solid-state reactions [10], co-precipitation [11, 12], sol–gel [13–15], and so forth. The electrochemical performance of electrode materials is strongly influenced by synthesis methods. $LiNi_{0.5}Mn_{1.5}O_4$ spinel material prepared by solid-state method produces larger particles of irregular shape, poor control of stoichiometry, and so on. $LiNi_{0.5}Mn_{1.5}O_4$ spinel material prepared by sol–gel method can produce highly homogeneous, smaller particles with good crystallinity while it requires high calcination temperature. Co-precipitation process also can produce small particles with uniform particle distribution and good crystallinity, but the whole synthesis route is complicated and time-consuming.

One-dimensional nanofibers constructed with nanoparticle subunits can effectively keep the contact areas large and fully realize the advantage of nanosized active materials. Zheng

✉ Ling Wu
lwu@suda.edu.cn

[1] School of Iron and Steel, Soochow University, Suzhou 215021, China

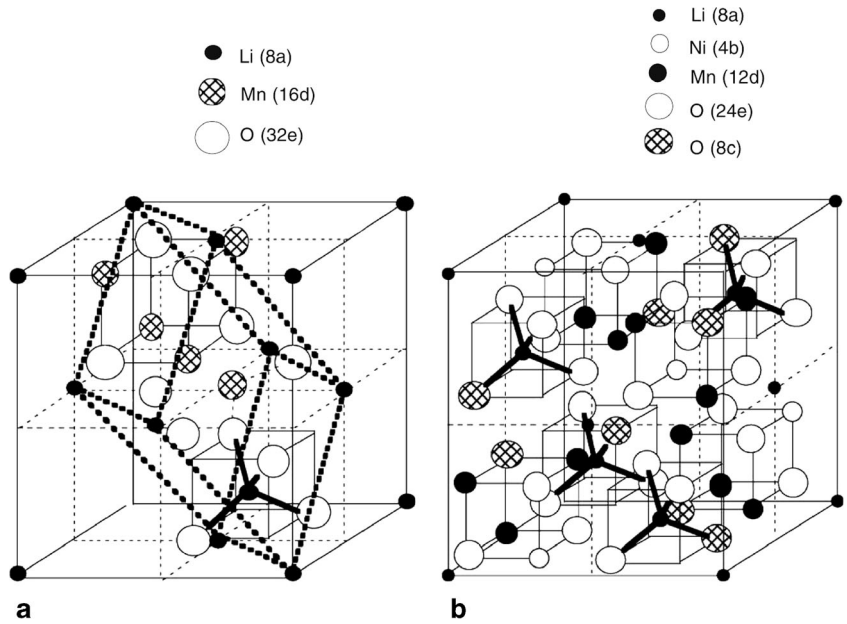

Fig. 1 Crystal structure diagram of $LiNi_{0.5}Mn_{1.5}O_4$ in two different space groups. **a** Face-centered spinel (Fd3m); **b** primitive simple cubic ($P4_332$) [22]

et al. [16, 17] have successfully synthesized nanosheets and microspheres of VPO_4/C, the conclusion shows. The VPO_4/C nanosheets deliver a much higher electrochemical performance than the VPO_4/C microsphere does, which can be attributed to the nanosheet structure. Increasing the interfacial reaction area between the active material and the electrolyte and decreasing the Li-ion diffusion length in the active material both contribute to a high Li insertion–extraction rate [18]. Fibers can be obtained by electrospinning process; the as-prepared electrospinning nanofibers of $LiNi_{0.5}Mn_{1.5}O_4$ were expected to improve its electrochemical properties due to its small particles and short diffusion distance of lithium-ion [19]. However, electrospinning technique was seldom used to produce nanostructured $LiNi_{0.5}Mn_{1.5}O_4$. Xu et al. [20] have successfully prepared $LiNi_{0.5}Mn_{1.5}O_4$ cathode material by the electrospinning method, and his point is about the impact on morphology of different heating rates. Liu et al. [21] have also successfully prepared $LiNi_{0.5}Mn_{1.5}O_4$ cathode material by the electrospinning method, and his point is about the advantage of this method. The electrochemical performance of the sample synthesized by the electrospinning method is better than the sample synthesized by the common poly(vinyl pyrrolidone) powder (PVP)-assisted sol–gel method. In this paper, the $LiNi_{0.5}Mn_{1.5}O_4$ cathode material has been successfully prepared by an electrospinning method and the different electrochemical performances due to unequal annealing temperatures are investigated. The formation of $LiNi_{0.5}Mn_{1.5}O_4$ fibers of submicron or nanometer size is thought to enhance electrochemical performance by reducing the transport path lengths of lithium ions and electrons. In addition, decreasing the

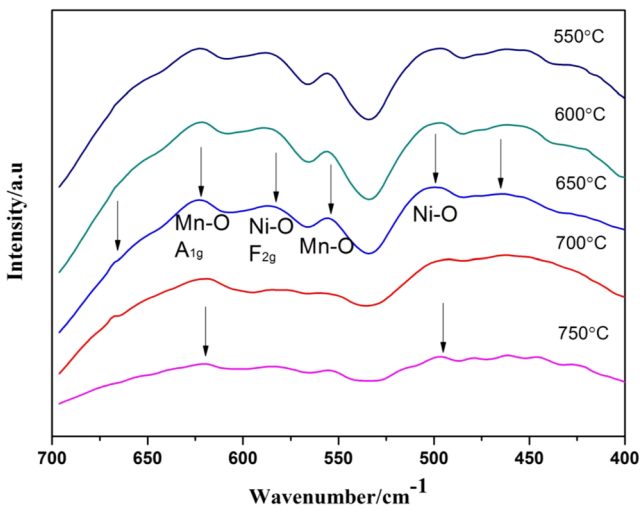

Fig. 2 FTIR curves of $LiNi_{0.5}Mn_{1.5}O_4$ synthesized at different temperatures

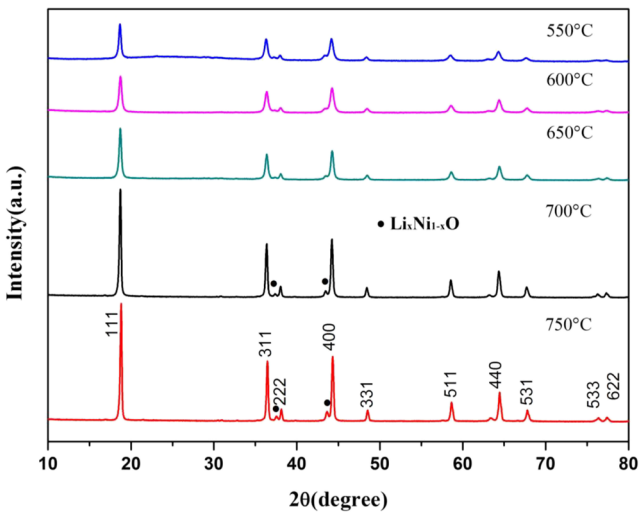

Fig. 3 XRD patterns of $LiNi_{0.5}Mn_{1.5}O_4$ synthesized at different temperatures

Table 1 Lattice parameters and crystallite size of $LiNi_{0.5}Mn_{1.5}O_4$ synthesized at different temperatures

Temperature (°C)	a (Å)	D_{111} (nm)
550	0.8173	20.5
600	0.8176	23.8
650	0.8179	24.2
700	0.8180	31.2
750	0.8182	34.6

crystallite size is important for the electrode–electrolyte interface and may also reduce the mechanical lattice strain upon Li insertion/extraction [21].

Experimental

$LiNi_{0.5}Mn_{1.5}O_4$ was prepared by an electrospinning method using lithium hydroxide, manganese acetate, nickel acetate, acetic acid, ethanol, and poly(vinyl pyrrolidone) as the starting materials. Firstly, 0.42 g $LiOH{\cdot}H_2O$, 3.68 g $Mn(CH_3COO)_2{\cdot}4H_2O$, and 1.24 g $Ni(CH_3COO)_2{\cdot}4H_2O$ were dissolved in 18 g acetic acid and then the solution was heated to 80 °C under constant magnetic stirring, which was named S1. Secondly, 8 g PVP (Mw = 1,300,000) was dispersed in 100 ml ethanol, to prepare the solution named S2, and then 18 g S2 was added into S1. The mixed solution was further stirred at room temperature to get the uniform sol.

The as-obtained spinnable sol was loaded into a plastic syringe equipped with a needle tip. A positive terminal was connected to the tip. The as-synthesized nanofibers were collected in an aluminum foil. The distance between the tip and the collector was 15 cm and the applied voltage was 12 kV. The aluminum foil covered with nanofibers was dried in an oven at 80 °C for 6 h. The nanofibers were sintered at 550–750 °C for 3 h under air atmosphere to obtain the $LiNi_{0.5}Mn_{1.5}O_4$ samples.

Vertex 70 (Bruker Co., Germany) was used for Fourier transform infrared (FTIR) study. The phase analysis of the samples was conducted via X-ray diffraction (XRD, X'Pert Pro) using Cu Kα radiation scanning in the range of 10° to 80° (2θ). The morphology of the samples was observed by scanning electron microscope (SEM, JSM-6380 LV).

The electrochemical characterizations were performed using a CR2025 coin-type cell. The positive electrodes were fabricated from 10 wt.% acetylene black, 10 wt.% polyvinylidene fluoride (PVDF) binder, and 80 wt.% active material. The blended slurries were pasted onto an aluminum

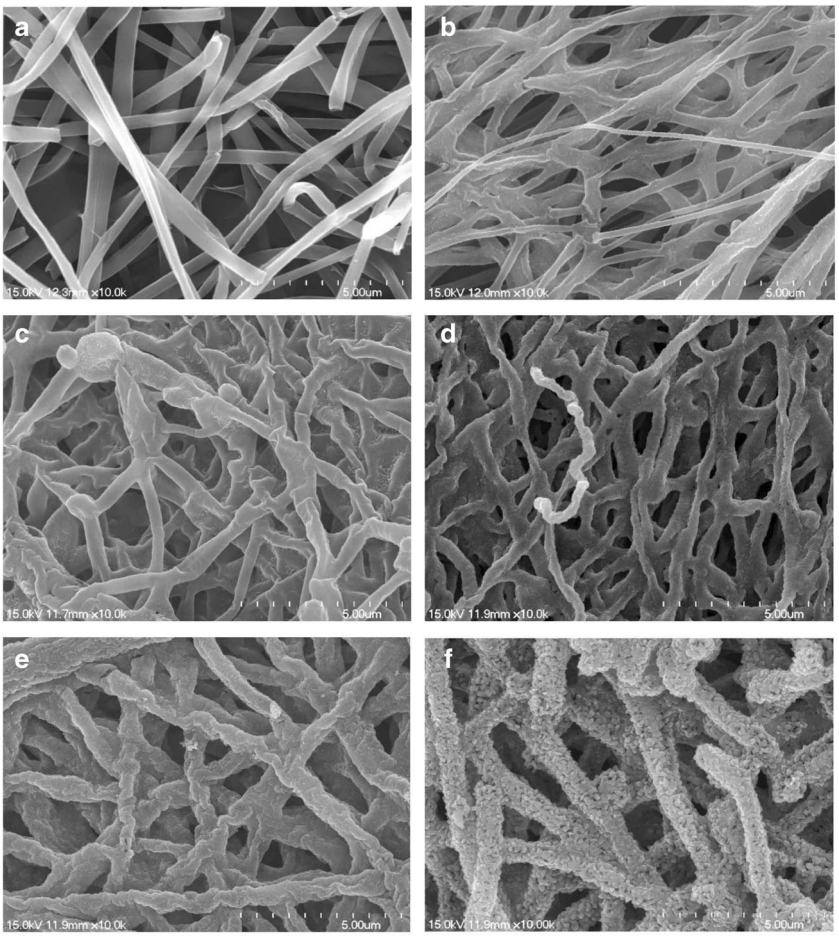

Fig. 4 SEM images of the precursor and $LiNi_{0.5}Mn_{1.5}O_4$ samples synthesized at different temperatures. **a** Precursor nanofibers; **b** 550 °C; **c** 600 °C; **d** 650 °C; **e** 700 °C; **f** 750 °C

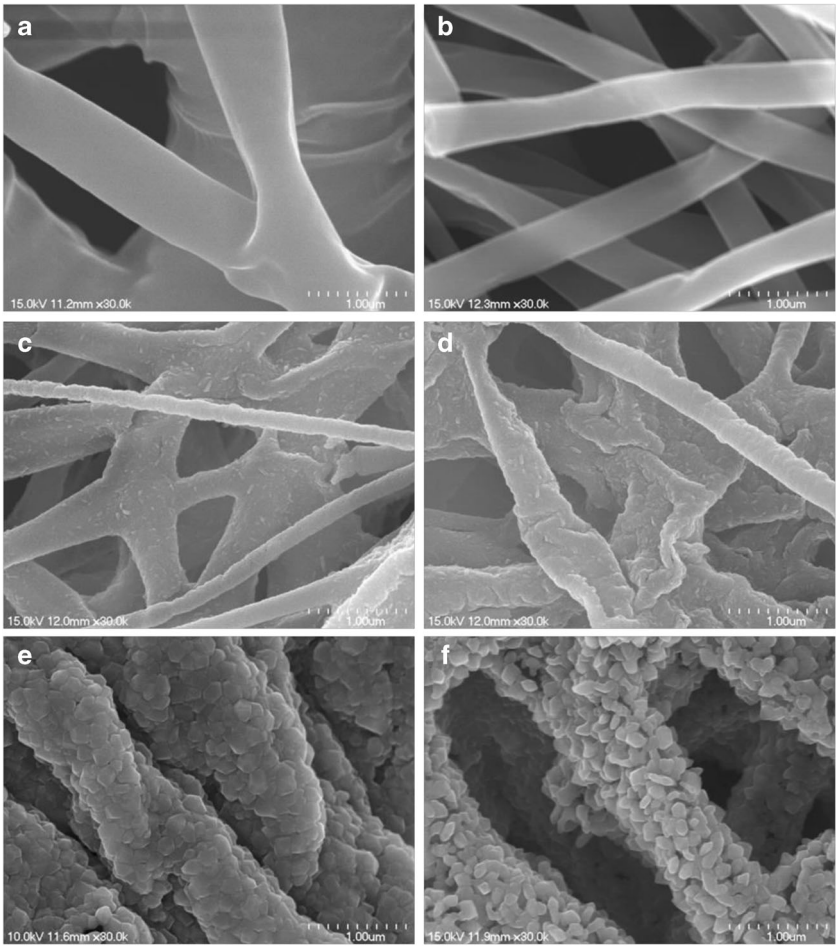

Fig. 5 The high-magnification SEM images of the precursor and $LiNi_{0.5}Mn_{1.5}O_4$ samples synthesized at different temperatures. **a** Precursor nanofibers; **b** 550 °C; **c** 600 °C; **d** 650 °C; **e** 700 °C; **f** 750 °C

current collector, dried at 120 °C for 4 h in vacuum. Then, the cells were assembled in an argon-filled glove box with $LiNi_{0.5}Mn_{1.5}O_4$ as the cathode, Li metal as the anode, and 1 M $LiPF_6$ solution in a mixture of ethylene carbonate and dimethyl carbonate with a volumetric ratio of 1:1 as the electrolyte. The cells were charged and discharged in the voltage range of 3.0–4.9 V at room temperature. The cyclic voltammetry tests (CV) and electrochemical impedance spectroscopy (EIS) tests were performed with a CHI660D electrochemical work station. The CV curves for the above test cells were recorded in the potential range of 3–5 V, and EIS experiments were carried out in the frequency range of 0.01 ~ 100 kHz.

Results and discussion

It is known that the $LiNi_{0.5}Mn_{1.5}O_4$ spinel has two different space groups, the transition metal ordered $P4_332$(P-type) and the cation disordered Fd3m(F-type). Figure 1 shows the crystal structure diagram of the two different space groups [22]. Because of the similar scattering factors of Ni and Mn, the structural difference between these two space groups is hardly to be observed by XRD. FTIR spectra were used to distinguish P-type and F-type. Figure 2 shows the FTIR spectra of $LiNi_{0.5}Mn_{1.5}O_4$ sintered at different temperatures. For the samples sintered below 650 °C, at least six absorption bands can be observed in the range of 450–700 cm^{-1}. However, for the samples sintered at 750 and 700 °C, only two broad absorption bands are observed. The strong band around 620 cm^{-1} could be related to the symmetric Mn–O stretching mode of MnO_6 octahedral (A_{1g}), and the peak at about 500 cm^{-1} could be caused by the Ni^{2+}–O stretching mode in the structure. The peaks at about 560 and 580 cm^{-1} are mainly due to the ordering location of Ni/Mn atoms. The split of the band at 550–600 cm^{-1} implies the ordered structure of the spinel structure [12]. The $LiMn_{1.5}Ni_{0.5}O_4$ sintered below 650 °C shows $P4_332$ structure. In the ordered $P4_332$ structure, $Ni^{2+}$and Mn^{4+} ions occupy octahedral 4a and 12b sites of the spinel lattice, respectively, while these cations distribute randomly on the octahedral 16d sites in the disordered Fd3m structure [23]. Many researchers reported that the rate capability offered by disordered Fd3m, $LiNi_{0.5}Mn_{1.5}O_4$ spinels was much better than that of ordered $P4_332$ spinels due to the higher electronic and ionic conductivities [24].

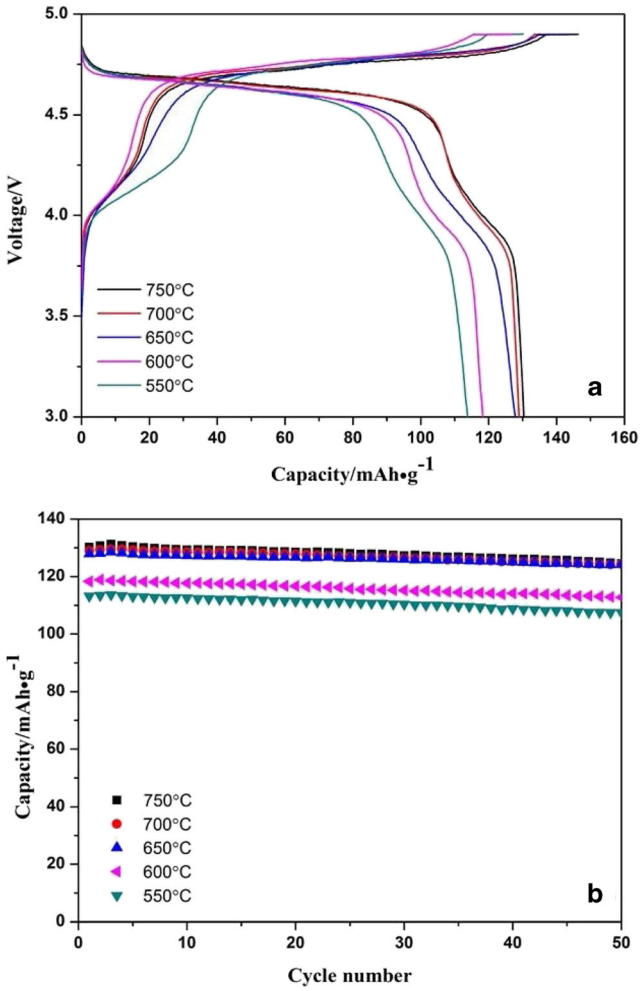

Fig. 6 **a** Initial charge–discharge curves and **b** cycling performance of $LiNi_{0.5}Mn_{1.5}O_4$ synthesized at different temperatures

In Fig. 3, the XRD patterns of the $LiNi_{0.5}Mn_{1.5}O_4$ samples sintered at different temperatures are presented. It is found that the as-prepared samples show the typical pattern of a cubic spinel. As the sintering temperatures increase from 550 to 750 °C, the diffraction peaks become sharper and stronger, indicating the improvement of crystallinity. It is noted that a small amount of $Li_xNi_{1-x}O$ impurities appeared in the patterns of the sample sintered at 700 °C. This is a common feature when the Ni content (x) in the $LiNi_xMn_{2-x}O_4$ spinel exceeds 0.2 % [25]. According to the previous report [26], $LiNi_{0.5}Mn_{1.5}O_4$ loses oxygen and disproportionate to a mixture of a spinel phase and a secondary phase $Li_xNi_{1-x}O$ because of partial reduction of Mn^{4+} to Mn^{3+} at a temperature above 650 °C. The preparation of pure phase of controlled stoichiometry of nickel and oxygen content in the $LiNi_{0.5}Mn_{1.5}O_4$ powders is difficult due to similarity in the ionic radii of Li and Ni ions, and cation disproportionate will happen, so we can also see small impurity peaks in the patterns of the sample sintered under 700 °C. The lattice parameters and crystallite size of the samples synthesized at different temperatures are listed in Table 1. Clearly, a growth of crystallites showing up followed with the increase of the sintering temperature.

The SEM images of the precursor and $LiNi_{0.5}Mn_{1.5}O_4$ samples synthesized at different temperatures are exhibited in Fig. 4. The precursor nanofibers had smooth surface covered by a layer of polymer with a diameter of 400–600 nm. The nanofibers were randomly oriented and interwoven like a spider's web. After sintering, the nanofibers remained randomly oriented and displayed an interwoven architecture, whereas their diameters decreased to 300–500 nm and the surfaces became rough (Fig. 4b–d). The reduction of the nanofiber size and the roughness of the surface were probably caused by the loss of polymer within the nanofibers. The high-magnification SEM images were provided in Fig. 5 to observe the surface change of $LiNi_{0.5}Mn_{1.5}O_4$ cathode materials after different high-temperature annealing. With the increasing of sintering temperature, the nanofibers' size increased. It was ascribed to the subunits' growth and aggregations. Such a structure should be very favorable for lithium storage as small particles as well as a short diffusion distance of lithium-ion owing to the nanoscale dimensions [21].

Figure 6 shows the initial charge–discharge curves and cycling performance of the samples at 0.1 C rate. It can be seen that the samples sintered at 750 °C exhibit the highest reversible initial discharge capacity of 130.3 $mAhg^{-1}$ and its coulombic efficiency is 89 %. However, the sample sintered at 650 °C shows the highest capacity retentions of 97.1 % after 50 cycles and a reversible initial discharge capacity of 127.8 $mAhg^{-1}$, which is close to the capacity of samples sintered at 750 °C. Its coulombic efficiency is also 89 %. All the curves show two plateaus with a high-voltage plateau of approximately 4.7 V and a low-voltage plateau of approximately 4.0 V. The high-voltage plateau can be ascribed to the two-step oxidation/reduction of Ni^{2+}/Ni^{3+} and Ni^{3+}/Ni^{4+}, while the low-voltage plateau can be attributed to the redox reaction of Mn^{3+}/Mn^{4+} couples [27]. To further investigate the electrochemical performance of $LiNi_{0.5}Mn_{1.5}O_4$, their rate capabilities are compared.

Figure 7a–e presents the charge–discharge curves of the samples at different rates. The discharge capacity of $LiNi_{0.5}Mn_{1.5}O_4$ sintered at 650 °C drops with increasing current density, from 127.8 $mAhg^{-1}$ at 0.1 C to 105 $mAhg^{-1}$ at 3 C, the coulombic efficiency decreases from 89 to 87 %, and the voltage plateau shifts from 4.7 to 4.1 V. The results were superior to those of other samples. The improved cycling performance and rate capacity can be partially attributed to the high electronic and ionic conductivity resulted from the small particles as well as a short diffusion distance of lithium-ion.

Figure 7f shows the cyclic stability of $LiNi_{0.5}Mn_{1.5}O_4$ samples at different rates. It can be seen that all the samples exhibit excellent cycling performance at low current rate. The sample sintered at 750 °C shows a discharge capacity of 127.9 and 97 mAh g^{-1} at 0.5 and 3 C rate, respectively, which are 98.2 and 75.4 % of its capacity at 0.1 C rate. The sample sintered at

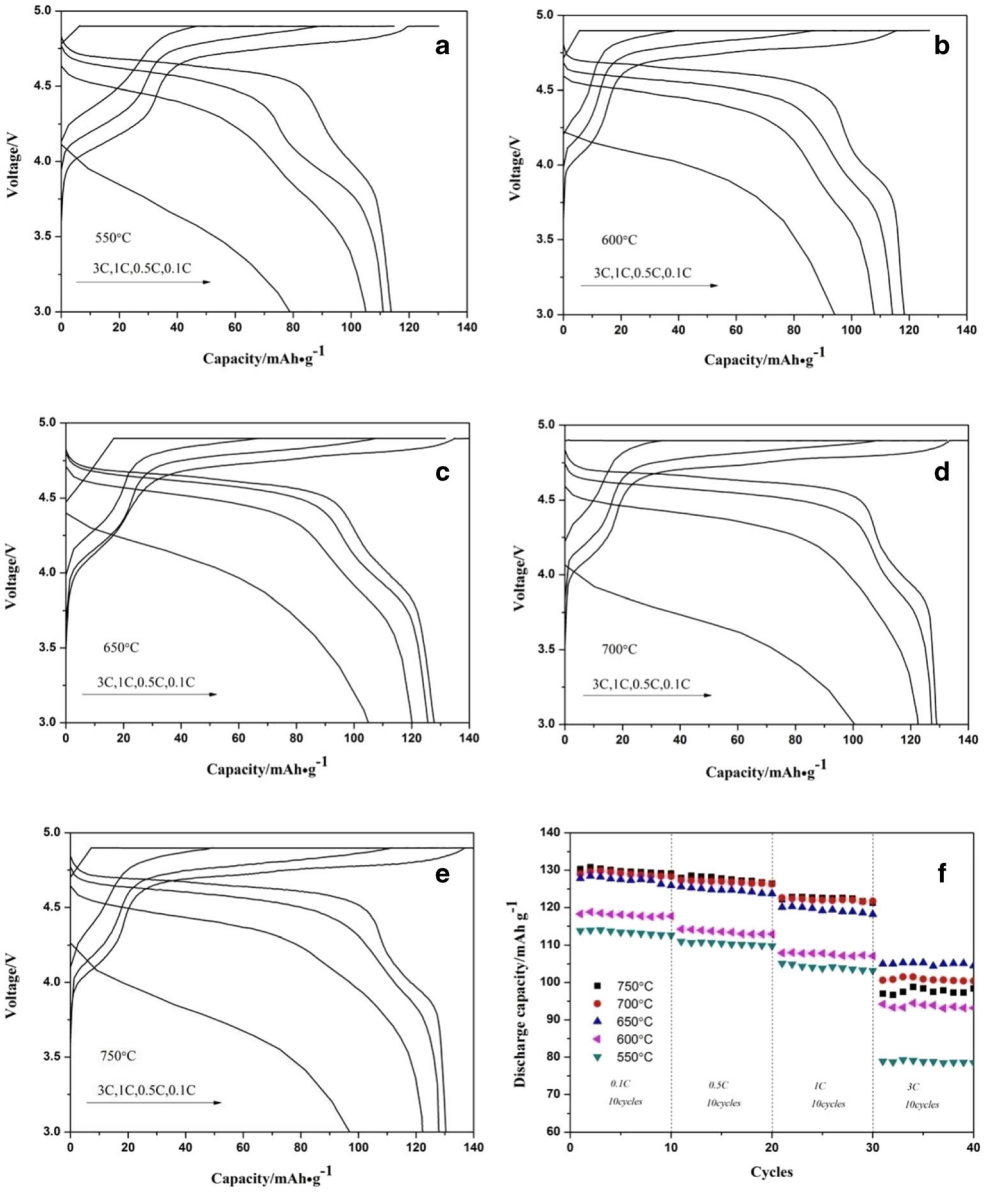

Fig. 7 The rate performances (**a**–**e**) and cycling performances (**f**) of $LiNi_{0.5}Mn_{1.5}O_4$ samples synthesized at different temperatures

650 °C shows a discharge capacity of 125.6 and 105 mAh g^{-1} at 0.5 and 3 C rate, respectively, which are 98.3 and 82.2 % of its capacity at 0.1 C rate. The significant difference in rate capability is observed at 3 C rate. The sample sintered at 650 °C exhibited much better electrochemical properties than did other samples, which was mainly because the fibers of the samples sintered at higher temperatures became large and aggregate, resulting in the increase of the charge transfer resistance (R_{ct}), and the reduction of the electrical conductivity of $LiNi_{0.5}Mn_{1.5}O_4$, which is consistent with the results of Fig. 8

Figure 8 shows the AC impedance spectra of electrodes made of different $LiNi_{0.5}Mn_{1.5}O_4$ samples. It can be seen that the fitting results are in good agreement with the experimental data, indicating that the equivalent circuit is reasonable. In the circuit, the *Rs* represents the ohmic resistance of the electrolyte and electrode, as the intercept impedance on the z-axis. The CPE1

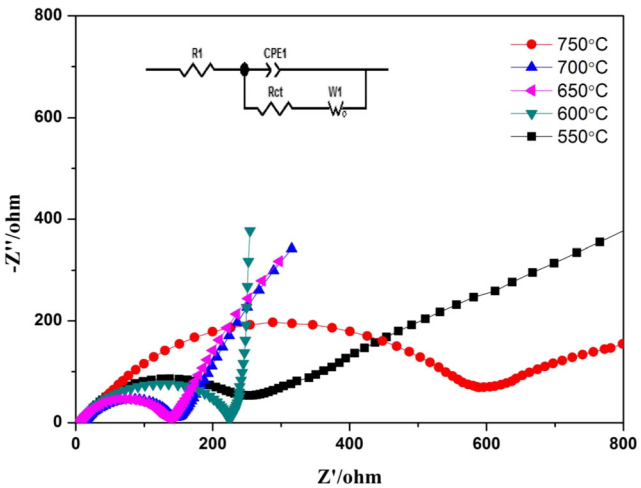

Fig. 8 AC impedance spectra of electrodes made of different $LiNi_{0.5}Mn_{1.5}O_4$ samples and their corresponding equivalent circuit

Table 2 Impedance parameters of $LiNi_{0.5}Mn_{1.5}O_4$ synthesized at different temperatures

Temperature (°C)	R_s (Ω)	R_{ct} (Ω)
750	14.89	407.2
700	11.2	132.7
650	6.3	122.3
600	10.71	180.9
550	7.99	211.3

represents the double layer capacitance, a parameter to fit the testing data. The *Rct* represents the charge transfer resistance of electrochemical reaction, and the W1 represents the diffusion-controlled Warburg impedance. According to the equivalent circuit, the diameter of the semicircle represents the sum of the film resistance of Li^+ diffusion and charge transfer resistance. The parameters of the equivalent circuit are shown in Table 2. It is found that the charge transfer resistance of the sample sintered at 650 °C (122.3 Ω) is much lower than that of the sample sintered at 750 °C (407.2 Ω), indicating that the electrical conductivity of the sample sintered at 650 °C is higher than that of the sample sintered at 750 °C. According to Fig. 5, the nanofibers of the sample sintered at 650 °C are smooth and interwoven like a spider's web, while the nanofibers of the sample sintered at 750 °C are rough and fractured. It is clear that the sample sintered at 650 °C has a smaller polarization and Li^+ diffuses easier. They result in the lower charge transfer resistance.

In Fig. 9, the cyclic voltammetry curve of the $LiNi_{0.5}Mn_{1.5}O_4$ cathode is exhibited. The sweep rate is 0.05 mV/s and the sweep voltage is 3.5–5 V. As shown, there are three oxidation peaks in the potential range of 3.5–5 V, which are in agreement with the charge/discharge curves (Fig. 6). The two oxidation peaks near 4.8 V are induced by a successive increase of Ni ionicity, $Ni^{2+} \rightarrow Ni^{3+}$ and $Ni^{3+} \rightarrow Ni^{4+}$, respectively. The cathode exhibits small redox peaks near 4 V which are attributable to Mn^{3+}/Mn^{4+} redox. The potential differences between cathodic and anodic peaks are 0.24 and 0.29 V, respectively. These results

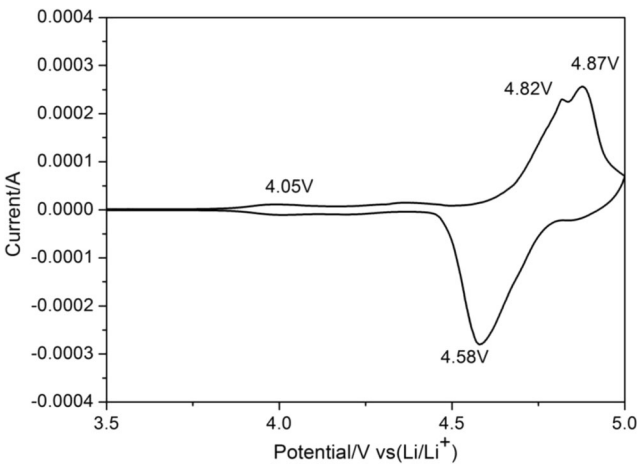

Fig. 9 CV curves of $LiNi_{0.5}Mn_{1.5}O_4$ synthesized at 650 °C (sweep rate 0.05 mV/s; sweep voltage 3.5–5 V)

indicate that the $LiNi_{0.5}Mn_{1.5}O_4$ cathode possesses a small polarization and has a good cycling performance.

Conclusion

$LiNi_{0.5}Mn_{1.5}O_4$ cathode material can be successfully synthesized by electrospinning. The synthesized sample shows a nanofiber shape and that the average size is about 300–500 nm. The sample sintered at 650 °C exhibits the best electrochemical property. The initial discharge capacity of the sample is 127.8 mAh g^{-1} at 0.1 C rate and exhibits good rate capability and cycling performance. Because of the short diffusion distance and small particles, the electronic and ionic conductivity can be improved. The as-prepared nanofibers of $LiNi_{0.5}Mn_{1.5}O_4$ exhibits remarkably better electrochemical performance compared with octahedron shape.

Acknowledgments The study was sponsored by the National Natural Science Foundation of China (51574168, 51574170, and 51404156).

References

1. Amatucci G, Tarascon JM (2002) Optimization of insertion compounds such as $LiMn_2O_4$ for Li-Ion batteries. J Electrochem Soc 149:K31–K46
2. Ding YL, Xie J, Cao GS, Zhu TJ, Yu HM, Zhao XB (2011) Single-crystalline $LiMn_2O_4$ nanotubes synthesized via template-engaged reaction as cathodes for high-power lithium ion batteries. Adv Funct Mater 21:348–355
3. Yuan GH, Bai JT, Doan TNL, Chen P (2014) Synthesis and electrochemical investigation of nanosized $LiMn_2O_4$ as cathode material for rechargeable hybrid aqueous batteries. Mater Lett 137:311–314
4. Talik E, Lipinska L, Zajdel P, Zalog A, Michalska M, Guzik A (2013) Electronic structure and magnetic properties of $LiMn_{1.5}M_{0.5}O_4$ (M=Al, Mg, Ni, Fe) and $LiMn_2O_4/TiO_2$ nanocrystalline electrode materials. J Solid State Chem 206:257–264
5. Liu W, Liu J, Chen KF, Ji SM, Wan YL, Zhou YC, Xue DF, Hodgson P, Li YC (2013) Enhancing the electrochemical performance of the $LiMn_2O_4$ hollow microsphere cathode with a $LiNi_{0.5}Mn_{1.5}O_4$ coated layer. Chem Eur J 20:824–830
6. Xiang MW, Ye LQ, Peng CC, Zhong L, Bai HG, Su CW, Guo JM (2014) Study on the electrochemical performance of high-cycle $LiMg_{0.08}Mn_{1.92}O_4$ cathode material prepared by a solid-state combustion synthesis. Ceram Int 40:10839–10845
7. Bhaskar A, Bramnik NN, Trots DM, Fuess HM, Ehrenberg H (2012) In situ synchrotron diffraction study of charge–discharge mechanism of sol–gel synthesized $LiM_{0.5}Mn_{1.5}O_4$ (M=Fe, Co). J Power Sources 217:464–469
8. Santhanam R, Rambabu B (2010) Research progress in high voltage spinel $LiNi_{0.5}Mn_{1.5}O_4$ material. J Power Sources 195:5442–5451
9. Lin HB, Zhang YM, Hu JN, Wang YT, Xing LD, Xu MQ, Li XP, Li WS (2014) $LiNi_{0.5}Mn_{1.5}O_4$ nanoparticles: synthesis with synergistic effect of polyvinylpyrrolidone and ethylene glycol and performance as cathode of lithium ion battery. J Power Sources 257:37–44
10. Hagh NM, Amatucci GG (2010) A new solid-state process for synthesis of $LiMn_{1.5}Ni_{0.5}O_{4-\delta}$ spinel. J Power Sources 195:5005–5012

11. Zhang MH, Liu YZ, Xia YG, Qiu B, Wang J, Liu ZP (2014) Simplified co-precipitation synthesis of spinel $LiNi_{0.5}Mn_{1.5}O_4$ with improved physical and electrochemical performance. J Alloys Compd 598:73–78
12. Zhu Z, Zhang D, Yu HY (2014) Preparation of spherical hierarchical $LiNi_{0.5}Mn_{1.5}O_4$ with high electrochemical performance by a novel composite co-precipitation method for 5V lithium ion secondary batteries. Electrochim Acta 115:290–296
13. Xu HY, Xie S, Ding N, Liu BL, Shang Y, Chen CH (2006) Improvement of electrochemical properties of $LiNi_{0.5}Mn_{1.5}O_4$ spinel prepared by radiated polymer gel method. Electrochim Acta 51: 4352–4357
14. Hwang BJ, Wu YW, Venkateswarlu M, Cheng MY, Santhanam R (2009) Influence of synthesis condition on electrochemical properties of high-voltage $Li_{1.02}Ni_{0.5}Mn_{1.5}O_4$ spinel cathode material. J Power Sources 193:828–833
15. Liu W, Liu J, Wan YL, Ji SM, Zhou YC (2013) Synthesis of $LiNi_{0.5}Mn_{1.5}O_4$ nano-and micropolyhedra via sol–gel method and their application for Li-ion batteries. Energy Environ Focus 2:68–72
16. Zheng JC, Han YD, Zhang B, Shen C, Ming L, Ou X, Zhang JF (2014) Electrochemical properties of VPO_4/C nano-sheets and microspheres as anode materials for lithium-ion batteries. ACS Appl Mater Interfaces 6:6223–6226
17. Zhang B, Han YD, Zheng JC, Zhang JF, Shen C, Ming L, Yuan XB, Li H (2014) $VOPO_4$ nanosheets as anode materials for lithium-ion batteries. Chem Commun 50:11132–11134
18. Hosono E, Saito T, Hoshino J, Mizuno Y, Okubo M, Asakura D, Kagesawa K, Nishio-Hamane D, Kudoa T, Zhou HS (2013) Synthesis of $LiNi_{0.5}Mn_{1.5}O_4$ and $0.5Li_2MnO_3$–$0.5LiNi_{1/3}Co_{1/3}Mn_{1/3}O_2$ hollow nanowires by electrospinning. CrystEngComm 15:2592–2597
19. Guan HY, Shao CL, Liu YC, Yu N, Yang XH (2004) Fabrication of $NiCo_2O_4$ nanofibers by electrospinning. Solid State Commun 131: 107–109
20. Xu R, Zhang XF, Chamoun R, Shui JL, Li JCM, Lu J, Amine K, Belharouak I (2015) Enhanced rate performance of $LiNi_{0.5}Mn_{1.5}O_4$ fibers synthesized by electrospinning. Nano Energy 15:616–624
21. Liu J, Liu W, Ji SM, Zhou YC, Hodgson P, Li YC (2013) Electrospun spinel $LiNi_{0.5}Mn_{1.5}O_4$ hierarchical nanofibers as 5V cathode materials for lithium-ion batteries. ChemPlusChem 78:636–641
22. Amdouni N, Zaghib K, Gendron F, Mauger A, Julien CM (2007) Magnetic properties of $LiNi_{0.5}Mn_{1.5}O_4$ spinels prepared by wet chemical methods. J Magn Magn Mater 309:100–105
23. Zhong GB, Wang YY, Zhang ZC, Chen CH (2011) Effects of Al substitution for Ni and Mn on the electrochemical properties of $LiNi_{0.5}Mn_{1.5}O_4$. Electrochim Acta 56:6554–6561
24. Kunduraci M, Amatucci GG (2008) The effect of particle size and morphology on the rate capability of 4.7V $LiMn_{1.5+\delta}Ni_{0.5-\delta}O_4$ spinel lithium-ion battery cathodes. Electrochim Acta 53:4193–4199
25. Ein-Eli Y, Vaughey JT, Thackeray MM, Mukerjee S, Yang XQ, McBreen J (1999) $LiNi_xCu_{0.5-x}Mn_{1.5}O_4$ spinel electrodes, superior high-potential cathode materials for Li batteries: I. electrochemical and structural studies. J Electrochem Soc 146:908–913
26. Fang HS, Wang ZX, Zhang B, Li XH, Li GS (2007) High performance LiNi0.5Mn1.5O4 cathode materials synthesized by a combinational annealing method. Electrochem Commun 9:1077–1082
27. Li DC, Ito A, Kobayakawa K, Noguchi HY, Sato YC (2007) Electrochemical characteristics of $LiNi_{0.5}Mn_{1.5}O_4$ prepared by spray drying and post-annealing. Electrochim Acta 52:1919–1924